A method for cross-comparison of scatterometer data using natural distributed targets: application to ERS-1 and ERS-2 data during the tandem mission

Anis Elyouncha and Xavier Neyt

Royal Military Academy, Brussels, Belgium

ABSTRACT

A methodology of cross-comparison of C-band spaceborne scatterometers is developed and applied to ERS-1 and ERS-2 scatterometers data. Assuming the differences between the instruments can be represented by an incidence-angle dependent bias, this paper presents and discusses four methods providing an estimate of that bias and of its standard deviation. These methods use natural distributed targets such as rainforest, ocean and sea ice, and are based on geophysical model functions, namely constant gamma model, CMOD5 and sea ice line model. The backscatter from the natural distributed targets is compared against a simulated backscatter provided by the models. Finally, the deviation of the two datasets from the models are compared to yield a bias between the two scatterometers. The methodology is applied to ERS-1 and ERS-2 data acquired during the tandem mission in 1996. Generally, the bias between the ERS-1 and ERS-2 scatterometers is smaller than 0.2 dB over most incidence angles and the four methods provide relatively consistent results. However, in order to achieve a consistent backscatter data, the scatterometers need to be inter-calibrated. The methodology can be useful to cross-calibrate scatterometers on-board other satellites (e.g. METOP, OceanSat-2, HY2A, etc.) in the view of the Global Climate Observing System guidelines.

Keywords: Scatterometer calibration, Ocean calibration, ERS-1, ERS-2

1. INTRODUCTION

Since the launch of the European Remote sensing Satellite ERS-1, a continuous measurement of backscattering signal has been acquired by the scatterometers on-board the two satellites ERS-1, ERS-2. Over the ocean, this backscatter (normalized radar cross-section) or σ_0 (sigma nought), is used to determine the wind speed and direction.[1] Over land, many applications using the σ_0 have emerged,[2] one of the best known application over land is the soil moisture retrieval.[3] Over sea ice, σ_0 is used to discriminate between open water and sea ice[4,5]

The importance of long-term, continuous, and homogeneous satellite data is strongly encouraged by the international scientific community.[6] Therefore, cross-comparison and inter-calibration of different instruments has become essential to meet this objective.

The AMI (in wind mode) instrument on board ERS-1 and ERS-2 are scatterometers designed to obtain accurate measurement of the backscatter from the surface of the Earth.

There are many reports on the calibration of scatterometers, see,[7],[8],[9,10] and[11] to cite a few. There are however very few reports on the cross-comparison of two scatterometers considering datasets acquired during the same time period, see[12] for instance which compares ERS-2 and ASCAT using collocated backscatter and soil moisture.

While most of these papers concentrate on a single calibration method, several calibration methods exist. These methods can broadly be characterized by the fact that the measured sigma nought is converted to an intermediate value (typically, a geophysical value such as wind speed, ice age or gamma nough) using a model. That intermediate value is then compared to known references. There are various assumptions associated with the model and the reference values used, mainly related to temporal stability. The difference between the intermediate value and the known reference is

Further author information: (Send correspondence to Anis Elyouncha) E-mail: anis.elyouncha@rma.ac.be, Telephone: +32 2 737 6665, Address: Signal and Image Center, Electrical Engineering Dept, Royal Military Academy, 30 av de la Renaissance, B-1000 Brussels, Belgium

usually linked to a gain offset in the instrument as this is considered as the most prominent source of calibration error*. That gain offset is assumed to be linear and incidence angle dependent as one of the main source of gain change is the antenna radiation diagram. The underlying assumption is that those gain changes in time are due to the aging of the (electronic) components and deformation of the antenna.

In this paper, we propose to discuss and compare several methods to perform the cross-comparison of scatterometer instruments. The comparisons are performed on data acquired in the same time period, which relaxes the requirements on the temporal stability of the model and of the reference values. Moreover, as we consider a cross-comparison of the instruments, we are not that much interested in the bias (the difference between the measurement and the modeled value using the known reference) but by the difference in bias between the compared instrument. The methods are illustrated using ERS-1, ERS-2 data.

This paper is organized as follows. Section II gives an overview of the missions and the instruments. The datasets are described in the section III. Section IV is dedicated to the methodology of the cross-comparison, it describes each method, the related distributed target, the associated model and the assumptions made. The results are reported in Section V. The conclusions are included in the last section.

2. MISSION AND INSTRUMENT DESCRIPTION

The first European remote sensing satellite (ERS-1) of the European Space Agency (ESA) was launched on July 17, 1991 into a Sun-synchronous polar orbit. The scatterometer on-board ERS-1 (AMI) provided observations on winds in operational mode until June 03, 1996. ERS-1 failed on March 10, 2000, exceeding its expected lifespan. ERS-2 was launched in April 1995 as the follow-on mission to ERS-1. The ERS-2 scatterometer operated from November 1995 to July 2003 in global mission. The recorders on-board failed on June 22, 2003. Since then until the end of the mission (July 2011), the instrument operated only within the visibility of the ground stations (regional scenario). Consequently, the coverage of the Brazilian rainforest, used as a distributed target for calibration monitoring purposes was strongly degraded. The ERS-1/ERS-2 missions (simultaneous operation) overlapped during 9 months from August 17, 1995 to June 03, 1996.

During the so called tandem mission, ERS-1 and ERS-2 were flying in the same orbital plane with an inclination of about 98.5 degrees to the Earths equatorial plane. Both satellites were flying at the same mean altitude of 785 km, providing a repeat cycle of 35 days. With the nominal orbital configuration, ERS-2 followed ERS-1 with an approximate delay of 35 min. Because of this delay and the Earths rotation, the ground-track patterns of ERS-2 were shifted westwards with respect to those of ERS-1. The orbit phasing has been adjusted to ensure that ERS-2s track over the Earths surface coincides exactly with that of ERS-1 24 h earlier.[13]

ERS-1 and ERS-2 carried an Active Microwave Instrument (AMI). The AMI is a real aperture radar operating at a frequency of 5.3 GHz (C-Band) and using three vertically polarized antennas. The AMI has three modes of operation, namely the Image Mode, the Wave Mode, and the Wind Mode. It uses three sideways looking antennas, one looking to the right side of the satellite track (mid beam antenna), one looking forward at 45 azimuth projection angle with respect to the mid beam (fore beam antenna), and one looking backward at 45 azimuth projection angle with respect to the mid beam (aft beam antenna). The three beams illuminate a 500 km wide swath as the satellite moves along its orbit.[14, 15]

3. DATASETS

The backscatter and associated information (angles, flags, etc.) are extracted from BUFR products which contain the level 1b calibrated backscatter values. The products used are in nominal resolution i.e., 25 km between adjacent nodes or Wind Vector Cells (WVC). ERS-2 offer also products with higher resolution (12.5 km).

The dataset covers a period of two months and a half (from 20th March 1996 to 3rd June 1996) during the tandem mission. The datasets for the different methods are summarized in Tables 1.

*The authors note that other non-gain related calibration issues may exist such as geometry-related or noise-power related. These issues are not considered in this paper.

Method	Test area	Time period
Collocation	Global (Collocations are found above 80^o)	From 20/03/1996 to 03/06/1996
Ocean	Global ocean [90S-90N, 180W-180W]	From 20/03/1996 to 03/06/1996
Rainforest	Amazon [15S-5N, 75W-55W]	From 20/03/1996 to 03/06/1996
Sea ice	Arctic sea ice [50N-90N, 180W-90E]	From 20/03/1996 to 03/06/1996

Table 1. ERS-1/ERS-2 cross-comparison dataset

4. CROSS-COMPARISON METHODOLOGY

The methodology developed in this work is a set of cross-comparison methods applicable on natural distributed targets (e.g., rainforest, ocean and sea ice) which are associated to geophysical models and assumptions. Several natural regions of known properties have been studied using scatterometer data[16,17] and several empirical backscatter models have been developed.[18–22] The main principle of these methods is a comparison of the measured backscatter and a simulated backscatter computed using the considered geophysical model. Each method provides an incidence-angle dependent bias between the two data sets (instruments) and is assessed by its standard deviation. Additionally, a direct comparison of the collocated data (in time, distance and geometry) is performed.

The compared satellites fly on similar orbits and the on-board instruments operate at the same central frequency and operating principles. The differences in backscatter between the instruments measurements are assigned to a difference in their antenna gain diagram. Therefore, the quantities calculated in this paper (geophysical parameters and biases) are resolved per antenna and incidence angle.

Diurnal variations of σ_0 over the Amazon forest have been observed.[23–25] Therefore, the measurements are processed and presented separately for ascending and descending passes. The convention applies to other methods too.

In the following sub-sections, each method is described. The considered target properties, the model and the assumptions are also detailed.

4.1. Cross-comparison using collocated measurements

This method is based on the comparison of near simultaneous observations of the same area on the ground by the two scatterometers. The conditions for collocation are as follows: 1) maximum distance between pairs of WVC is 12.5 km, 2) maximum difference in time is 60 minutes, 3) maximum difference in incidence angle is 1^o, 4) maximum difference in azimuth angle is 5^o. And the underlying assumptions are that the radar backscatter is temporally stable over short time intervals, and spatially homogeneous over short distances. In practice, the maximum difference in time is 33 min and the maximum difference in incidence angle is 0.2^o.

Due to the configuration of the orbits, most collocated measurements are found at high latitudes near the North pole. For instance, for the collocation conditions listed above, all the tandem mission collocations are found above 80^o latitude.

The result of this comparison method is a bias between the two instruments which is obtained by averaging the differences between the collocated measurements. This bias is defined as

$$Bias(\theta) = E[{\sigma_0}^{ERS-1}(\theta) - {\sigma_0}^{ERS-2}(\theta)]. \quad (1)$$

4.2. Cross-comparison over the rainforest

The rainforest is assumed to be homogeneous, stable in time and isotropic at C-band frequency.[23,24] Given these assumptions, the σ_0 depends only on incidence angle. The incidence angle dependence can be removed by using the parameter γ_0 defined by

$$\gamma_0 = \sigma_0 / cos(\theta) \quad (2)$$

where θ is the incidence angle

The rainforest ([15S-5N],[75W,55W]) was shown to exhibit spatial inhomogeneities and that these could be removed by using a spatial mask.[11] Roughly, a mask is built by excluding areas having a very low or a very high γ_0.

SIR (Scatterometer Image Reconstruction) product, derived from NSCAT, is used to select dense forest.[26] The selected area is illustrated in figure 1 left. As can be seen, the spatial mask removes rivers and de-forested (urban) areas. It can be noticed (figure 1 right) that there is a difference between the ascending and descending γ_0 distributions. This difference is due to the diurnal effect mentioned earlier.

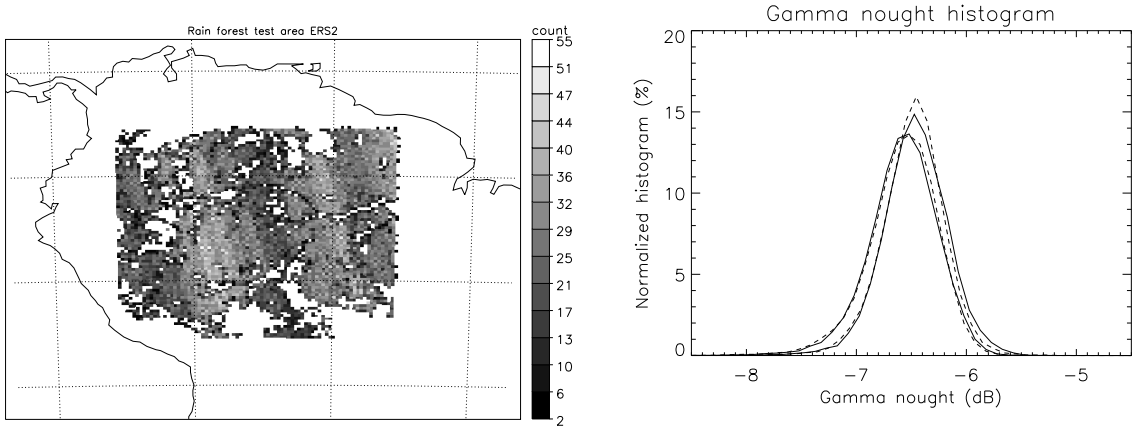

Figure 1. Rainforest data (left), Gamma nought histogram (right) - solid line: ERS-1, dashed line: ERS-2

For each instrument, γ_0 is computed and averaged over the (masked) rainforest. The averaged γ_0 of one scatterometer is compared to the averaged γ_0 of the other scatterometer. The bias between the two instruments is then given by

$$Bias(\theta) = E[{\gamma_0}^{ERS-1}(\theta)] - E[{\gamma_0}^{ERS-2}(\theta)]. \tag{3}$$

4.3. Cross-comparison over the ocean

A series of C-band GMFs (e.g., CMOD4,[21] CMOD5[27] and CMOD5.n[28,29]) relating σ_0 to the equivalent neutral wind vector at 10m height have been developed empirically and successively improved using satellite scatterometer data. The representation of these models in the σ_0 measurement space looks like a double cone.[30] The model considered in this paper is CMOD5 and is defined by

$$\sigma_0 = B0(\theta,V)[1 + B1(\theta,V)cos\phi + B2(\theta,V)cos2\phi]^{1.6} \tag{4}$$

where θ is the incidence angle, V is the wind speed, φ is the wind direction and $B0$, $B1$, $B2$ are coefficients depending on θ and V.

The Numerical Weather Prediction (NWP)-based ocean calibration (NOC) method[8] is used. The procedure is briefly summarized hereafter, for a detailed description see.[31] The wind speed and direction for each measured σ_0 are obtained from the NWP winds. From this wind speed and wind direction, a simulated σ_0 (${\sigma_0}^{sim}$) is computed using (4). The distance between the measured σ_0 (${\sigma_0}^{meas}$) and ${\sigma_0}^{sim}$ is then computed. These distances are then averaged over the wind directions and then over the wind speeds. For practical reasons the wind speeds and directions are binned into bins of respectively 2 ms^{-1} and 10 degrees. In this work, ECMWF real winds are used with the CMOD5 model. The input winds are extracted from the BUFR products and the CMOD5 model is used to obtain ${\sigma_0}^{sim}$. This ${\sigma_0}^{sim}$ is then converted to z space using $z = (\sigma_0)^{0.625}$ before the NOC computation. This transformation from σ_0 space to z space is recommended by[1] and.[31]

The average difference between the measured z^{meas} and the simulated z^{sim} yields a model bias $Bias_m$, which is computed for each scatterometer as

$$Bias_m(\theta) = E[z^{meas}(\theta) - z^{sim}(\theta)]. \tag{5}$$

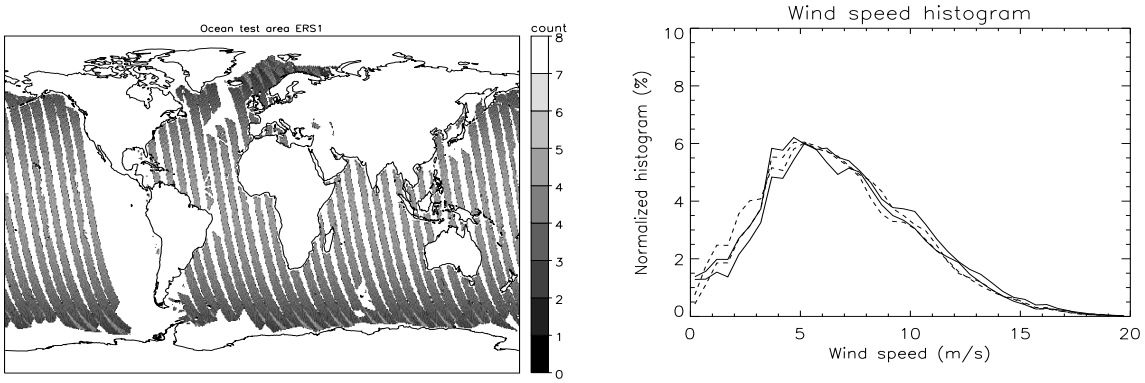

Figure 2. Ocean data (left), Wind speed histogram (right) - solid line: ERS-1, dashed line: ERS-2

The pair of model biases are then compared over the common incidence angle range. The bias between the two instruments is the difference between the two model biases

$$Bias(\theta) = Bias_m^{ERS-1}(\theta) - Bias_m^{ERS-2}(\theta). \tag{6}$$

4.4. Cross-comparison over sea ice

The backscatter triplets measured on sea ice depend on incidence angle and linearly on sea ice condition (ice age). The sea ice model[5] initially developed to discriminate between open water and sea ice backscatter triplets, is used here as a basis for cross-comparison. That model is given by

$$\sigma_0{}^{theo}(\theta, a) = \overline{\sigma_0}(\theta) + a e_a(\theta) \tag{7}$$

where $\overline{\sigma_0}$ and e_a depend on θ and a is the ice-line parameter.

The test area is restricted to a region above 70^o latitude around the North Pole. For each measurement $\sigma_0{}^{meas}$, the incidence angle is determined and used to compute the ice age parameter. IFREMER sea ice concentration product, derived from SSM/I, is used to select regions with ice concentration greater than 95 percent. Only measurements having a distance to the ice model less than 1 dB and positive ice age parameter a are considered. A map showing the ice age a from ERS-2 data averaged over all incidence angles and over the whole dataset is depicted in figure 3 for April 1996.

Using a a simulated backscatter $\sigma_0{}^{sim}$ is computed using (7). For each instrument, a bias with respect to the geophysical model is determined as

$$Bias_m(\theta) = E[\sigma_0{}^{meas}(\theta) - \sigma_0{}^{sim}(\theta)]. \tag{8}$$

The bias between the two instruments is the difference between the two model biases

$$Bias(\theta) = Bias_m^{ERS-1}(\theta) - Bias_m^{ERS-2}(\theta) \tag{9}$$

4.5. Assessment of the method

The bias provided by each method is considered as a random variable and the variance of that random variable is used to assess the reliability of the method. Owing to the complexity of the underlying models, it is not deemed possible to obtain an analytic expression the variance of each comparison method. Instead, the variance is empirically obtained as follows. Separately for each instrument, the WVCs are randomly assigned to n groups. n is selected so each packet of data contains a minimum number of measurements per incidence angle bin and per beam. n was chosen here equal to 10. All the methods are based on averaging the backscatter (or the related geophysical parameter), over groups of WVC falling in the same incidence-angle bin and the same beam. The bias between pairs of groups corresponding to two different instruments is computed yielding a set of n^2 biases. The bias and variance (standard deviation) of this set of biases is then computed.

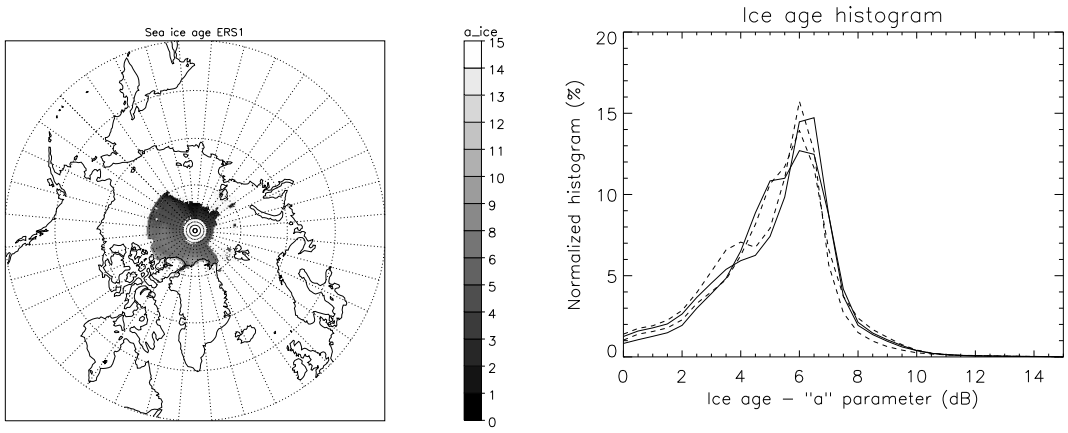

Figure 3. Sea ice data (left), ice age parameter histogram (right) - solid line: ERS-1, dashed line: ERS-2

5. RESULTS

This section summarizes the results of the four cross-comparison methods (ocean cross-comparison, sea ice cross-comparison, rainforest cross-comparison and cross-comparison based on the collocation) obtained by their application on two scatterometers. Figures 4 and 5 show the bias for the ERS-1/ERS-2 cross-comparison, respectively for ascending and descending passes.

There is a relatively good agreement between the methods presented. The four methods provide relatively consistent bias pattern (differing slightly in value). The direct comparison provides the highest bias, particularly noticeable at near range in the side beams figures. Note that, the incidence angle difference equals 0 for the mid beam for all the 19 nodes, while for the side beams $\Delta\theta$ can reach 0.2 deg. All the results show a small bias between ERS-1 and ERS-2 suggesting a calibration mismatch of approximately 0.1 dB with variations up to few 10th of dB, thus a need for inter-calibration.

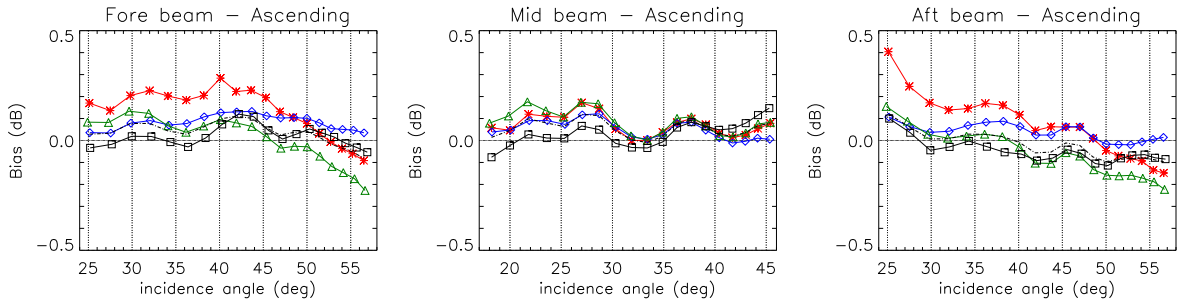

Figure 4. Red: Collocation, Blue: Ocean, Black: Sea ice , Green: Rainforest - Fore (left), Mid (center), Aft (right) - Ascending passes - April-June 1996

Table 2 shows that the biases between ERS-1 and ERS-2 provided by the four methods are very close and vary between -0.06 and 0.12 dB. The bias shown in the table are the average over incidence angle. These small biases suggest a reasonable inter-calibration of the two scatterometers, though an additional inter-calibration is needed to meet the Global Climate Observing System requirements. The standard deviation values are also very close with higher values for the collocation method.

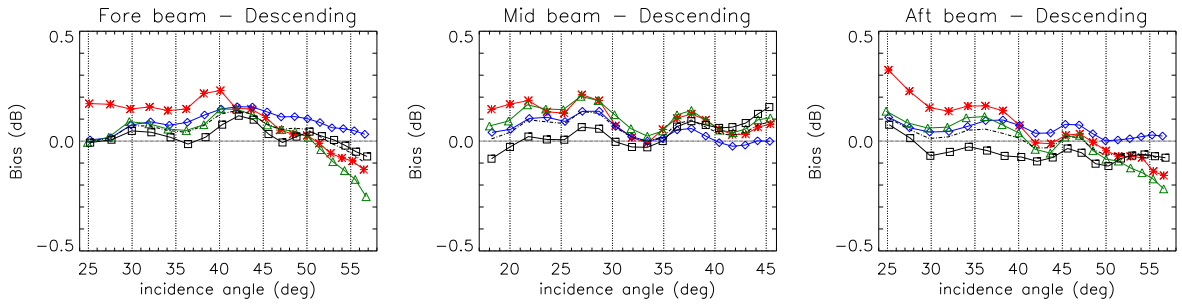

Figure 5. Red: Collocation, Blue: Ocean, Black: Sea ice , Green: Rainforest - Fore (left), Mid (center), Aft (right) - Descending passes - April-June 1996

Method	N (ERS-1)	N (ERS-2)	Bias (dB)			StDev (dB)		
Ascending passes			Fore	Mid	Aft	Fore	Mid	Aft
Ocean	4.235 M	3.516 M	0.082	0.048	0.036	0.010	0.009	0.010
Sea ice	0.859 M	0.638 M	0.155	0.130	0.099	0.012	0.009	0.012
Rainforest	123.5 K	99.55 K	0.002	0.089	-0.066	0.017	0.016	0.017
Collocation	14.46 K	14.46 K	0.128	0.069	0.066	0.056	0.031	0.053
Descending passes			Fore	Mid	Aft	Fore	Mid	Aft
Ocean	3.971 M	3.408 M	0.087	0.044	0.048	0.009	0.007	0.009
Sea ice	0.804 M	0.520 M	0.164	0.121	0.108	0.014	0.011	0.014
Rainforest	54.41 K	44.57 K	0.015	0.106	-0.010	0.027	0.026	0.028
Collocation	17.90 K	17.90 K	0.081	0.098	0.047	0.047	0.022	0.060

Table 2. Comparison of the four methods

6. CONCLUSIONS

A methodology of cross-comparison of two space-borne scatterometers has been developed and presented. Generally, the model-based methods performed more accurately (based on their standard deviation) than a direct comparison of σ_0. The diurnal effect was observed over the rainforest with an increase of the bias of approximately 0.1 dB during descending passes compared to ascending passes. Over the other targets, a negligible diurnal effect was observed.

The methodology has been applied to compare ERS-1/ERS-2 during the tandem mission. The four methods provide a relatively consistent results, except the collocation method which provides larger positive bias at near swath for the side beams. Finally, There is a noticeable incidence-angle dependent bias between ERS-1 and ERS-2 with variations within 0.2 dB. Thus, in order to achieve a consistent dataset, it is recommended to inter-calibrate ERS-1 and ERS-2 scatterometers. Correction coefficients can be computed (by averaging the model-based methods bias) and applied to the two scatterometers.

ACKNOWLEDGMENTS

This work was performed under European Space Agency (ESA) contracts. We would like to thank the ESA for the use of data and the provision of industry-confidential information. This work would not have been possible without the help of Pascal Lecomte and Raffaele Crapolicchio from the European Space Agency/ESRIN.

REFERENCES

1. A. Stoffelen, *Scatterometry*. PhD thesis, University of Utrecht, Oct. 1998.
2. V. Naeimi and W. Wagner, “C-band scatterometers and their applications,” in *Geoscience and Remote Sensing New Achievements*, P. Imperatore and D. Riccio, eds., pp. 229–246, InTech, 2010.

3. W. Wagner, *Soil moisture retrieval from ERS scatterometer data*. PhD thesis, Vienna University of Technology, Nov. 1998.
4. X. Neyt, N. Manise, and M. Acheroy, "Enhanced neural-network based sea/ice discrimination using ERS scatterometer data," in *Proceedings of SPIE Remote Sensing of the Ocean, Sea Ice and Large Water Regions 2005*, **5977**, pp. 55–64, Sept. 2005.
5. S. de Haan and A. Stoffelen, "Ice discrimination using ERS scatterometer," tech. rep., KNMI, Sept. 2001.
6. World Meteorological Organization, *Systematic Observation Requirements for Satellite-based Products for Climate*, Sept. 2006. GCOS-107 / WMO/TD 1338.
7. D. G. Long and G. B. Skouso, "Calibration of spaceborne scatterometers using tropical rain forests," *IEEE Transactions on Geoscience and Remote Sensing* **34**, Mar. 1996.
8. A. Stoffelen, "A simple method for calibration of a scatterometer over the ocean," *Journal of atmospheric and oceanic technology* **16**, pp. 275–282, Feb. 1999.
9. M. H. Freilich, H. Qi, and R. S. Dunbar, "Scatterometer beam balancing using open-ocean backscatter measurements," *Journal of Atmospheric and Oceanic Technology* **16**, pp. 283–297, Feb. 1999.
10. J. Verspeek, A. Stoffelen, M. Portabella, A. Verhoef, and J. Vogelzang, "ASCAT scatterometer ocean calibration," in *Proceedings of the IEEE International Geoscience and Remote Sensing Symposium*, **5**, pp. 248–251, July 2008.
11. N. Manise, X. Neyt, and M. Acheroy, "Calibration strategy for ERS scatterometer data reprocessing," in *Proceedings of the SPIE: Remote Sensing of the Ocean, Sea Ice, and Large Water Regions*, **5977**, pp. 88–97, Sept. 2005.
12. Z. Bartalis, "ERS-ASCAT backscatter and soil moisture intercomparison first results," tech. rep., TU-Wien IPF, June 2009.
13. G. Duchossois and P. Martin, "ERS-1 and ERS-2 tandem operations," Tech. Rep. ESA Bulletin Nr. 83, Directorate for Observation of the Earth and Its Environment, ESA, Paris, 1995.
14. E. P. Attema, "The active microwave instrument on-board the ERS-1 satellite," in *Proceedings of the IEEE*, **79**, pp. 791–799, June 1991.
15. P. Lecomte, "The ERS scatterometer instrument and the on-ground procesing of its data," in *Proc. of a Joint ESA-Eumetsat Workshop on Emerging Scatterometer Applications*, pp. 241–260, (Noordwijk, The Netherlands), Nov. 1998.
16. R. G. Kennett and F. K. Li, "Seasat over-land scatterometer data, part I: Global overview of the Ku-band backscatter coefficientts," *IEEE Trans. Geoscience Remote Sensing* **27**, pp. 592–605, Sept. 1989.
17. R. G. Kennett and F. K. Li, "Seasat over-land scatterometer data, part II: Selection of extended area land-target sites for the calibration of spaceborne scatterometers," *IEEE Trans. Geoscience Remote Sensing* **27**, pp. 779–788, Nov. 1989.
18. A. Cavanié, "An empirical C-band backscatter model over Arctic sea ice from ERS-1 AMI-wind data," in *Proc. of a Joint ESA-Eumetsat Workshop on Emerging Scatterometer Applications*, pp. 99–106, (Noordwijk, The Netherlands), Nov. 1995.
19. J. Verspeek, A. Stoffelen, and S. de Haan, "C-band sea ice model," in *Proc of the 2004 Envisat and ERS symposium*, (Salzburg, Austria), Sept. 2004.
20. A. E. Long, "Towards a C-band radar sea echo model for the ERS-1 scatterometer," in *Proceedings of the 3rd International Colloquium on Spectral Signature*, **ESA SP-247**, pp. 29–34, Eur. Space Agency Spec. Publ, 1985.
21. A. Stoffelen and D. Anderson, "Scatterometer data interpretation: Estimation and validation of the transfer function CMOD4," *Journal of atmospheric and oceanic technology* **14**, pp. 1298–1313, Feb. 1997.
22. H. Hersbach, "CMOD5 an improved geophysical model function for ERS C-band scatterometry," tech. rep., ECMWF, Sept. 2002. ECMWF technical Memorandum 395.
23. R. Crapolicchio and P. Lecomte, "On the stability of Amazon rainforest backscattering during the ERS-2 scatterometer mission lifetime," in *Proc. of the 2004 Envisat and ERS Symposium*, (Salzburg, Austria), Sept. 2004.
24. R. Hawkins, E. Attema, R. Crapolicchio, P. Lecomte, J. Closa, P. J. Meadows, and S. K. Srivastava, "Stability of Amazon backscatter at C-band: Spaceborne results from ERS-1/2 and RADARSAT-1," in *Proc. of the CEOS SAR Workshop*, **ESA-SP450**, (Toulouse, France), Oct. 1999.
25. L. B. Kunz and D. G. Long, "Calibrating SeaWinds and quikSCAT scatterometers using natural land targets," *IEEE Geoscience and Remote sensing letters* **2**, pp. 182–186, Apr. 2005.

26. D. G. Long and P. Hardin, "Vegetation studies of the amazon basin using enhanced resolution seasat scatterometer data," *IEEE Transactions on Geoscience and Remote Sensing* **32**, pp. 449–460, Mar. 1994.
27. H. Hersbach, A. Stoffelen, and S. de Haan, "An improved C-band scatterometer ocean geophysical model function: CMOD5," *J. Geophys. Res.* , 2007.
28. H. Hersbach, "CMOD5.N a C-band geophysical model function for equivalent neutral wind," tech. rep., ECMWF, Apr. 2008. ECMWF technical Memorandum 554.
29. M. Portabella and A. Stoffelen, "On scatterometer ocean stress," *J. Atm. Oceanic Technol.* , pp. 368–382, 2009.
30. A. Stoffelen and D. Anderson, "Scatterometer data interpretation: Measurement space and inversion," *Journal of atmospheric and oceanic technology* **14**, pp. 1298–1313, Feb. 1997.
31. J. Verspeek, "Scatterometer calibration tool development," Tech. Rep. SAF/OSI/CDOP/KNMI/TEC/TN/163, KNMI, Mar. 2006.